Modeling of Sub-Millimeter Wave Coplanar Waveguide Graphene Switches

Panagiotis C. Theofanopoulos and Georgios C. Trichopoulos
School of Electrical Computer and Energy Engineering
Arizona State University
Tempe, AZ USA 85287
ptheofan@asu.edu and gtrichop@asu.edu

***Abstract*—We present a theoretical study on the performance of graphene-loaded coplanar waveguide switches for 5G and beyond applications. Therefore, we exploit the tunable properties of graphene to device cost-effective, large-scale, broadband sub-millimeter-wave switches. Given the sheet impedance of biased and unbiased graphene monolayers, the model provides the optimum switching ratio with respect to insertion loss, characteristic impedance of transmission line, and graphene geometry. Using measured graphene sheet resistance, we compute the optimum switching performance for series and shunt single-pole-single-though sub-millimeter-wave (220-330 GHz) switches.**

Keywords—Graphene, millimeter-wave, switches

I. Introduction

Dynamically reconfigurable, multi-element electrically-large apertures are attractive devices for millimeter and sub-millimeter-wave (sub-mmW) wireless communications in 5G and future generations [1]. The proliferation of traditional phased arrays topologies is hindered by the losses and complexity of the RF-front-end networks (e.g. Butler matrices, power dividers, and phase shifters). Alternatively, using antenna, or transmission line integrated switches, we can achieve aperture reconfiguration to enable arbitrary pattern beam synthesis. However, higher frequency RF switches exhibit limited bandwidth, high losses [2][3], and integration in larger arrays is challenging due to the associated costs of the on-wafer real estate.

Alternatively, graphene allows the cost-effective implementation of broadband devices, distributed in large apertures [4]-[7]. Most studies rely on theoretical models of carrier transport in graphene [4] or use low-frequency in-plane measurements [5][6]. However, sub-millimeter-wave on-wafer measurements demonstrate that the actual graphene performance is far from ideal. Namely, graphene sheet impedance can be tuned from 300 Ω/□ to 1500 Ω/□ using external biasing [7]. Yet, the achievable modulation depth, when graphene is embedded in a switching topology, can differ from the sheet impedance ratio. For example, in [5], measurements below 110 GHz of a coplanar waveguide (CPW) graphene switch are presented, demonstrating the switching performance does not exceed 2 dB. Conversely, in [6], a tunable graphene-based microstrip attenuator is measured up to 10 GHz, and the achieved switching performance is 3-5 dB. Therefore, it is important to understand the dependence of switching performance on design parameters, including characteristic impedance, graphene patch geometry, and sheet impedance.

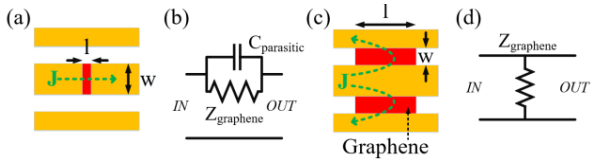

Fig. 1 Graphene switches in a coplanar waveguide (top view): (a) series and (c) shunt switches, with the respective equivalent circuits in (b) and (d). The dotted arrows indicate the electric current flow.

Hence, we classify graphene topologies into two categories: shunt and series (Fig. 1). For a CPW line, a series switch has a graphene patch integrated on the center conductor; in a shunt switch configuration, graphene is integrated between the signal and the ground conductors. Similar topologies can be designed for other types of transmission lines (e.g. microstrip).

II. Modeling of Graphene CPW Switches

To study the performance of the CPW graphene switches we consider the series and shunt graphene patches as lumped components, since, we assume that the longest graphene dimensions are significantly smaller than the guided wavelength. The S_{21} parameter determines the performance and state of the switch. For the CPW switch topology shown in Fig. 1, the S_{21} values are calculated from [8]

$$S_{21}^{series}=\frac{2}{2+Z_{sheet}/NZ_o},\quad S_{21}^{shunt}=\frac{2}{2+NZ_o/Z_{sheet}} \tag{1}$$

where Z_o is the characteristic impedance of the transmission line, Z_{sheet} is the graphene sheet impedance in Ω/□ (Ohms per square), and N is the number of graphene squares oriented in a line vertical to the current flow ($N_{series}=w/l$ and $N_{shunt}=l/w$).

The series (shunt) topology is in ON (OFF) state when the graphene is biased, thus leading to high (low) S_{21}. On the opposite, the series (shunt) switch is OFF (ON) when graphene is unbiased and the sheet resistance is high. The switching ratio (R) for each configuration is given by

$$R^{series}=\frac{2NZ_o+Z_{sheet}^{high}}{2NZ_o+Z_{sheet}^{low}},\quad R^{shunt}=\frac{Z_{sheet}^{high}\left(2Z_{sheet}^{low}+NZ_o\right)}{Z_{sheet}^{low}\left(2Z_{sheet}^{high}+NZ_o\right)} \tag{2}$$

The two switching performance metrics of interest are: i) insertion loss for the ON state and ii) the S_{21} ratio between the ON and OFF states. Observing the tradeoff between these metrics, we can identify the optimum design variables for our devices.

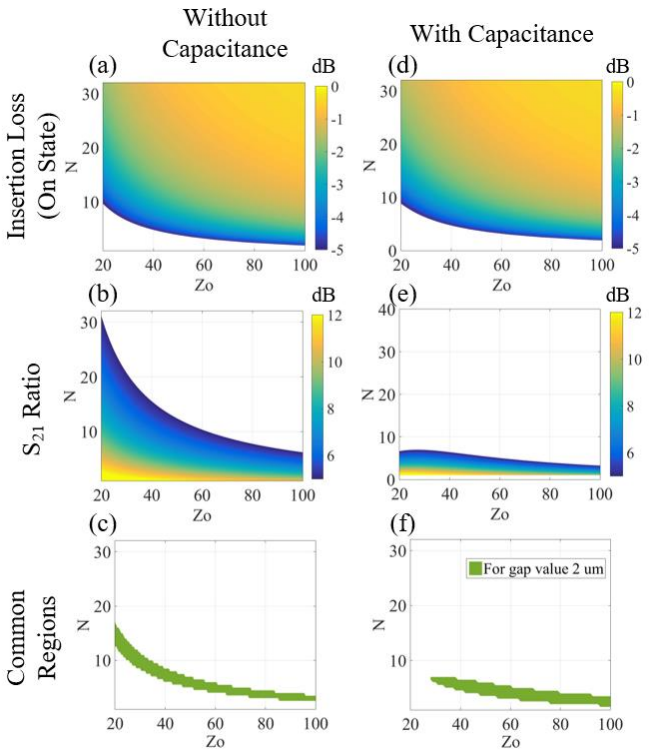

Fig. 2 The insertion loss, switching ratio, and (Z_o, N) combinations that meet the design specifications, for the CPW series graphene switch with and without the modeling of the parasitic capacitance.

III. Switching Performance with Respect to Design Parameters

In this section, we present simulation results for the CPW graphene switch configurations as a function of Z_o and N. As exemplary switching specifications, we set a maximum insertion loss of 5 dB and minimum switching ratio of 5 dB, as plotted in Figs. 2a-b. Because insertion loss and switching ratio are inversely proportional, only a fraction of the investigated (Z_o, N) combinations satisfy the specifications, as depicted in Fig. 2c.

However, graphene's inherently high sheet impedance poses restrictions to the series switch performance. To achieve lower impedance we need to use narrower patches, which creates a parallel RF path due to the parasitic capacitance. For that purpose, we model the same configuration at 300 GHz considering the coupling parasitic capacitance with a 2 μm gap [9]. As shown in Figs. 2d-e, the effect on the insertion loss is minimal; however, the switching ratio is severely affected, since the capacitor offers a better path for the current at the OFF state (high graphene impedance). For example, in Fig. 2f we observe that for $Z_o<30\ \Omega$ no (Z_o, N) combination meets the desired specifications.

For the shunt topology the insertion loss, switching ratio, and (Z_o, N) combinations for the same design specifications, are given in Fig. 3. Similarly, we identify the inverse proportionality of the insertion loss and the switching ratio as in the series topology. However, there is no limiting capacitance that compromises the shunt design as in the series case. Comparing Figs. 2f and 3c, the shunt topology allows for a larger range of (Z_o, N) combinations for the same design criteria.

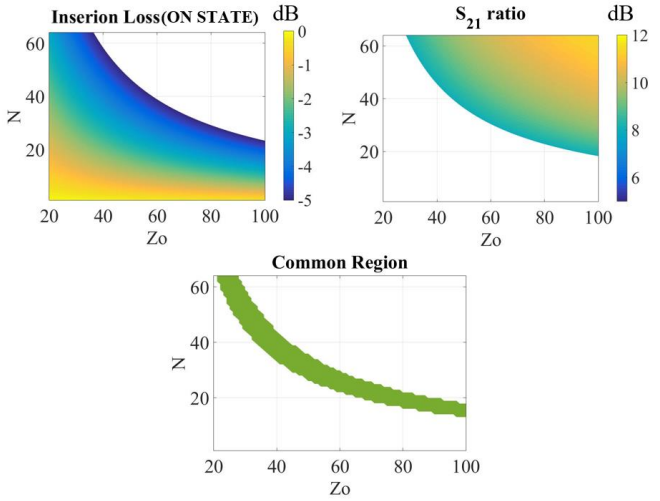

Fig. 3 The insertion loss, switching ratio, and (Z_o, N) combinations that meet the design specifications, for the CPW shunt graphene switch.

IV. Conclusions

Concluding, we presented preliminary results on the theoretical limitations of graphene-based CPW switches for the first time using measured graphene sheet impedances. Such switches enable the development of large-scale/multi-element dynamically reconfigurable apertures for 5G and beyond applications. The proposed methodology addresses the design of planar graphene-based switches and offers an insight into the expected performance. Finally, we plan to extend this study by incorporating various CPW gap dimensions, acquiring an in-depth understanding of the performance limitation of the proposed topologies.

References

[1] Y. Xing and T. S. Rappaport, "Propagation Measurement System and Approach at 140 GHz-Moving to 6G and Above 100 GHz," ArXiv eprints, Aug. 2018.

[2] J. Ajayan *et al.*, "InP high electron mobility transistors for submillimetre wave and terahertz frequency applications: A review," *AEU - Int. J. Electron. Commun.*, vol. 94, pp. 199–214, 2018.

[3] R. B. Yishay and D. Elad, "D-Band 360° Phase Shifter with Uniform Insertion Loss," *2018 IEEE/MTT-S International Microwave Symposium - IMS*, Philadelphia, PA, 2018, pp. 868-870.

[4] Y. Wu *et al.*, "A Generalized Lossy Transmission-Line Model for Tunable Graphene-Based Transmission Lines with Attenuation Phenomenon," *Sci. Rep.*, vol. 6, p. 31760, Aug. 2016.

[5] M. Dragoman *et al.*, "Coplanar waveguide on graphene in the range 40 MHz–110 GHz," *Appl. Phys. Lett.*, vol. 99, no. 3, p. 33112, Jul. 2011.

[6] L. Pierantoni *et al.*, "Broadband Microwave Attenuator Based on Few-Layer Graphene Flakes," in *IEEE Transactions on Microwave Theory and Techniques*, vol. 63, no. 8, pp. 2491-2497, Aug. 2015.

[7] N. Kakenov *et al.*, "Graphene-based terahertz phase modulators," *2D Mater.*, vol. 5, no. 3, p. 035018, May 2018.

[8] D. M. Pozar, Microwave Engineering, 2nd ed. New York, NY, USA: Wiley, 1998.

[9] R. N. Simons, *Coplanar waveguide circuits, components, and systems*. Cleveland: Wiley, 2009